



Gel polymer electrolyte based on hydrophilic–lipophilic TiO₂-modified thermoplastic polyurethane for high-performance Li-ion batteries

Yunhong Jiang¹, Feng Li¹, Yufan Mei¹, Yanhuai Ding^{1,*} , Huaji Pang², and Ping Zhang^{1,3,*}

¹Institute of Rheological Mechanics, Xiangtan University, Xiangtan 411105, Hunan, China

²School of Chemistry, Xiangtan University, Xiangtan 411105, Hunan, China

³National Engineering Center of Chemical Engineering Process Simulation and Enhancement, Xiangtan University, Xiangtan 411105, Hunan, China

Received: 18 June 2020

Accepted: 18 September 2020

Published online:

6 October 2020

© Springer Science+Business Media, LLC, part of Springer Nature 2020

ABSTRACT

Due to the advantages of high energy density and improved safety properties, Li metal batteries with gel polymer electrolyte (GPE) have drawn much attention in recent years. Herein, a novel gel thermoplastic polyurethane (TPU) electrolyte filled with ultrafine hydrophilic–lipophilic TiO₂ nanoparticles was successfully prepared by using a phase separation technology. The gel electrolyte can protect the battery against the leakage of liquid electrolyte by means of its strong interaction with Li⁺ and solvents. This kind of GPE shows an ionic conductivity of 1.59 mS cm⁻¹ and an electrochemical window of 4.3 V (vs. Li/Li⁺) at room temperature. Robust TiO₂ nanoparticles embedded into TPU matrix can effectively block dendrite puncture and, besides, greatly improve the thermal stability of GPE. The cycling performance, rate capability and mechanical properties guarantee the reliability of the as-prepared GPE in Li-ion batteries.

Introduction

Li-ion battery (LIB) has been recognized as an appealing power source due to its high energy density and long lifespan [1–8]. However, a rapid growth

of energy density, accompanied by an aggressive progress of volume reduction, brings serious safety concerns to LIBs [9–11]. Due to the high ionic conductivity and good compatibility with electrodes, liquid electrolytes have played indispensable roles in the field of electrochemical energy storage since the

Handling Editor: Kyle Brinkman.

Yunhong Jiang and Feng Li have contributed equally to this work.

Address correspondence to E-mail: yhding@xtu.edu.cn; zhangp@xtu.edu.cn

initial commercialization of LIBs more than 20 years ago [12–14]. However, the use of liquid electrolytes is plagued by a risk of leakage during the assembly and use [11, 15–17]. Besides, the uneven currents through the porous separators can induce the growth of lithium dendrite, especially for the use of lithium metal electrode [11, 16, 18, 19]. Thus, solid polymer electrolyte without liquid solvents has been considered as a very promising approach to address safety issues and restrain the dendrite growth [20, 21].

However, most of the solid polymer electrolytes exhibited low ionic conductivity (10^{-8} to 10^{-5} S cm⁻¹) and a poor compatibility toward the electrode, causing deterioration of cycling performance [12, 22]. The applications of solid polymer electrolyte were also restricted by its poor mechanical property. For this reason, gel polymer electrolytes (GPEs), incorporated the advantages of both liquid and solid electrolytes, have attracted considerable attention as they can function as not only separators but also electrolytes [23–26]. Besides, due to the processability of the polymer, GPEs can provide an adjustable shape and height flexibility for the energy storage device, which is promising for emerging portable and wearable electronic devices [26–28]. Furthermore, the flexible and elastic GPEs can tolerate the volume changes of the electrode materials during charging/discharging process [29–31]. Thus, GPEs have become one of the most ideal alternatives to various electrolytes for metal secondary batteries. In recent years, stretchable, flexible and multifunctional GPEs have been intensively studied [9, 32]. Song et al. summarized the methods for improving the mechanical and electrochemical properties of GPEs in the review paper [33]. Among them, exploring new polymer materials with low cost, high mechanical property and high absorption of liquid electrolyte has attracted much attention in recent years [34–36].

Generally, as the host materials, polymer matrix provides the GPEs with high mechanical integrity. Due to the high flexibility and spatial stability, thermoplastic polyurethane (TPU) possessed a two-phase microstructure which is a favorable host material for GPEs [37–40]. The soft phase in TPU can reduce the combination of the cations and anions and further boost the ion transportation in GPE; besides, the hard segments endow GPE with high strength and good film-forming capability [41–43]. Porous TPU/PVdF GPE prepared by electrostatic spinning method

showed superior electrochemical stability and good rate capacity in LIBs [41]. Nevertheless, it is still a challenge to prepare TPU-based GPEs with long-term cyclic stability. Compared with PVdF, hydrophilic–lipophilic anatase TiO₂ (ATO) is a promising alternative for developing TPU-based GPEs because of its high dielectric constant, good chemical and thermal stability [17, 24, 44]. In this study, we fabricated an advanced ATO-TPU GPE for LIBs. The as-prepared ATO-TPU composite polymer electrolytes show a wide electrochemical window, high lithium-ion transference number, remarkable cyclic stability and good rate capability in LIBs.

Experimental section

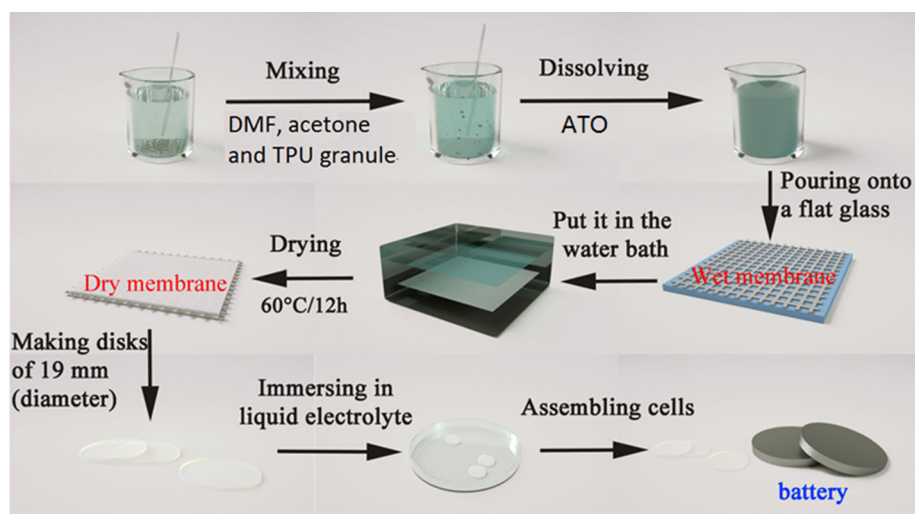
Materials

N,N-dimethylformamide (DMF, AR), acetone (AR), hydrophilic–lipophilic anatase TiO₂ (ATO) were purchased from Shanghai Macklin Biochemical Co., Ltd. TPU was purchased from Shanghai BASF Polyurethane Co., Ltd. Liquid electrolyte (1 M LiPF₆ in ethylene carbonate (EC)/dimethyl carbonate (DMC) = 1:1, v/v) was purchased from Suzhou Ganmin Chemical Reagent Co., Ltd. Commercial polypropylene (PP) separator was purchased from Celgard, China.

Preparation of ATO-TPU GPE

The preparation process of ATO-TPU GPE is shown in Scheme 1. ATO-TPU membrane was prepared by a phase inversion technique, and ATO-TPU GPE was further obtained by absorbing an amount of liquid electrolyte. In a typical procedure, 2.0 g TPU granule was dissolved in mixed solvents contained 10 ml DMF and 10 ml acetone. Then, 0.3 g ATO was dispersed into the solution at room temperature under vigorous stirring to form a transparent and viscous solution. The obtained solution was quickly cast onto a clean and flat glass plate and then immediately transferred into deionized water to complete the phase inversion process. After being dried at 60 °C for 12 h, the prepared membrane was immersed into a liquid electrolyte (1 M LiPF₆ in ethylene carbonate (EC)/dimethyl carbonate (DMC) = 1:1, v/v) for 1 h to form ATO-TPU GPE. The illustration of the phase inversion process is presented in Scheme 2. During

Scheme 1 The preparation process of ATO-TPU GPE.

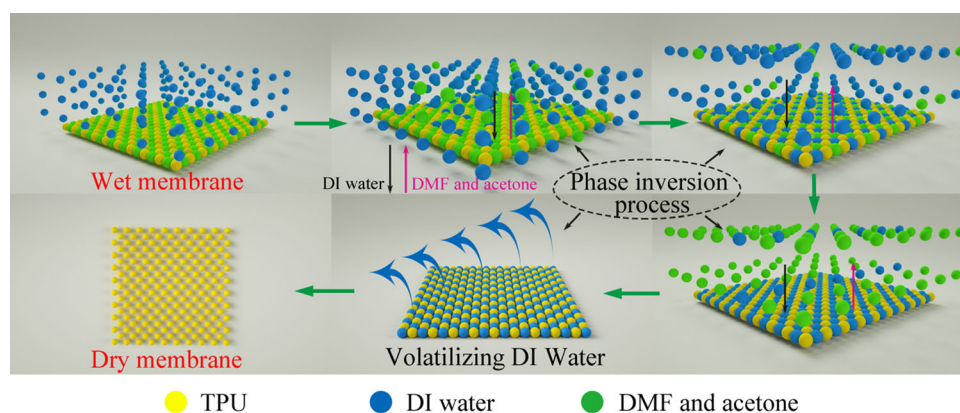


this process, the ATO-TPU membrane undergoes rapid diffusion between the organic solvents and non-solvent deionized water. The position of solvent molecules is gradually occupied by water molecules, and a wet and white ATO-TPU membrane is formed. When the membrane is dried at 60 °C, the water molecules in the membrane are slowly evaporated and small uniform pores are created. As a comparison, TPU GPE has been also prepared by the same procedure without ATO added. The thickness of all the GPE membranes was controlled at $\sim 56 \mu\text{m}$. More details related to the characterization of the materials and the electrochemical tests were provided in Supporting Information.

Results and discussion

XRD patterns and FTIR spectra of the samples are presented in Fig. 1. The FTIR spectra of PP, TPU and ATO-TPU in Fig. 1a show a series of characteristic absorption peaks in the whole wavenumber range $3900\text{--}600 \text{ cm}^{-1}$. The absorption peaks at 2915 cm^{-1} , 2845 cm^{-1} , 1465 cm^{-1} and 716 cm^{-1} are the stretching vibration of C-H bond in PP frame, indicating that commercial separator is polymerized from propylene. For the prepared TPU and ATO-TPU membranes, the FTIR spectra are the same kind, suggesting a weak effect of anatase TiO_2 on the structure of TPU. The characteristic absorption peaks that appeared at 3330 cm^{-1} can be assigned to the N-H groups in TPU chains; besides, the peaks at 1720 cm^{-1} and $1100\text{--}1280 \text{ cm}^{-1}$ are related to the vibration of C=O and C-O-C groups. Figure 1b presents the XRD analysis of ATO, ATO-TPU and TPU membranes. The XRD pattern of the TPU membrane

Scheme 2 The related illustrations of the phase inversion method.



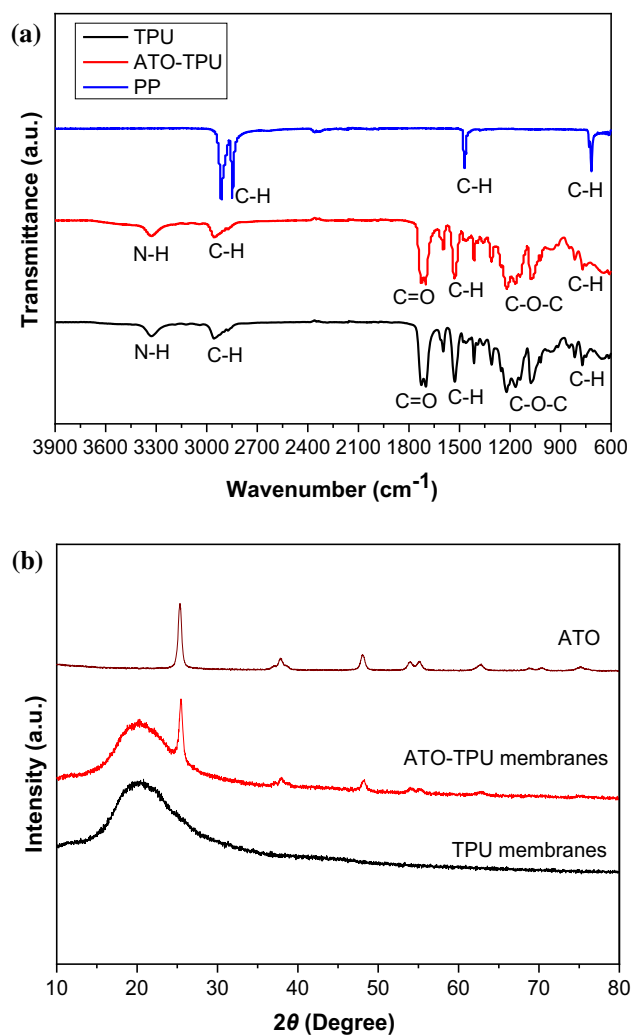


Figure 1 a FTIR spectra of PP, TPU and ATO-TPU membranes. b The XRD patterns of ATO, TPU and ATO-TPU membranes.

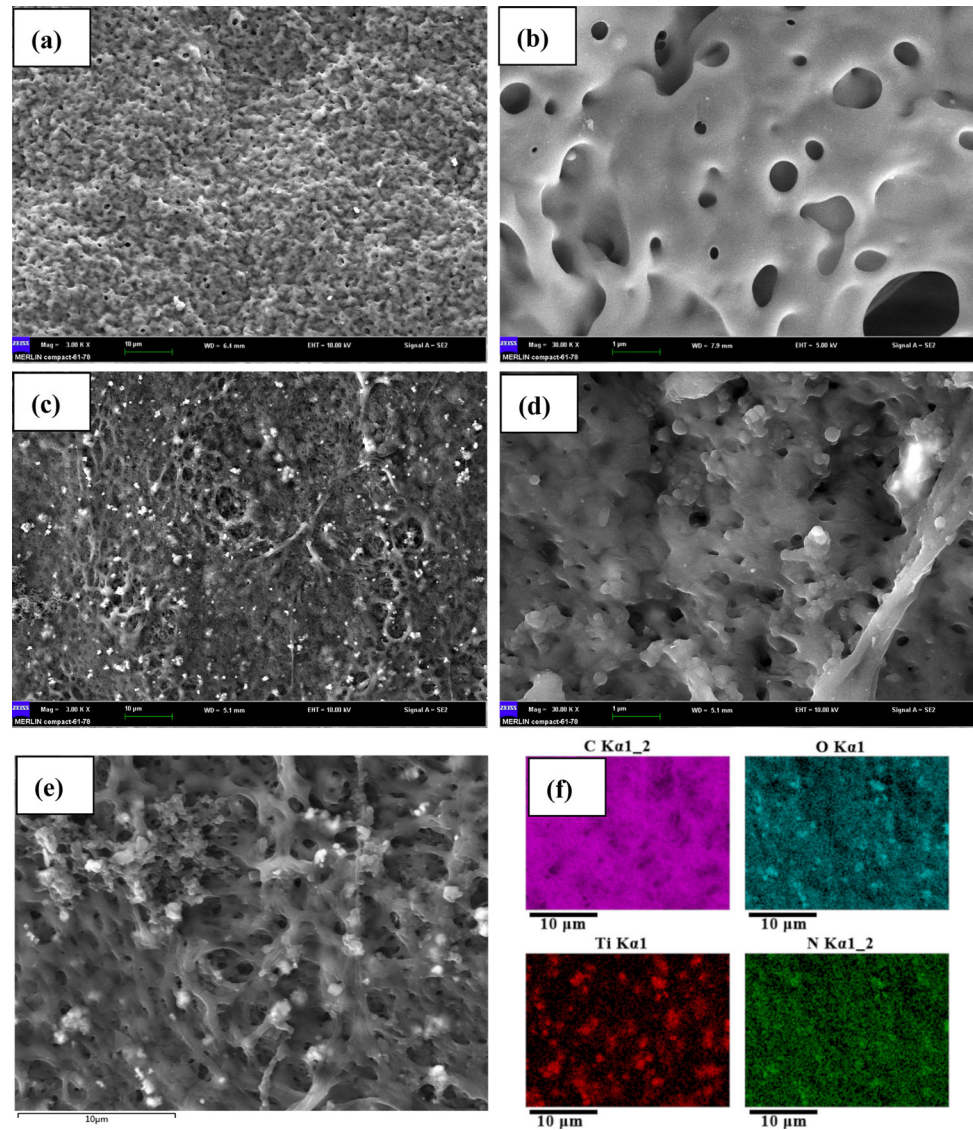
exhibits a broad peak at 2θ angles around 20° , indicating some degree of crystallinity. All the diffraction peaks of ATO can be assigned to anatase TiO_2 (JCPDS 89-4921). With the addition of ATO, the diffraction peak of ATO can be clearly observed in the XRD pattern of ATO-TPU membrane. Therefore, it is concluded that ATO-TPU composites are successfully prepared.

The pore structure determines the adsorbed amount of liquid electrolyte in GPEs. The surface morphologies of the TPU and ATO-TPU membranes were observed with scanning electron microscopy (SEM), as shown in Fig. 2a–d. A large number of pores can be observed on the surface of TPU and ATO-TPU membranes, which facilitates the uptake of liquid electrolyte in the polymer matrix. As shown in

Fig. 2a, b, in the absence of the ATO, the surface of the TPU membranes is smoother than that of the ATO-TPU membranes and the pores in the TPU membrane are large-sized and unevenly distributed, which is detrimental to the uptake of liquid electrolyte [25]. ATO nanoparticles can be readily identified in the SEM images of ATO-TPU membranes, which is in agreement with the XRD results. In order to further investigate the distribution of ATO nanoparticles, energy-dispersive X-ray (EDX) mapping analysis was performed. The analyzed area is presented in Fig. 2e, and the corresponding elements (C, O, Ti and N) mapping pictures are displayed in Fig. 2f. The uniform distribution of Ti and O over the entire area of the material indicates a successful distribution of ATO over the entire surface of the composite film.

Figure 3a shows the stress–strain profiles of the TPU and ATO-TPU membranes at room temperature. The TPU and ATO-TPU membranes show a tensile strength of 7.15 MPa and 19.20 MPa, with an elongation-at-break value at 340.86% and 408.33%, respectively. Although the tensile strength of the PP membrane reaches 108.52 MPa, however, the elongation at break is only 54.01% (Fig.S1a). Uniformly dispersed ATO nanoparticles constructed an inorganic framework in the ATO-TPU membrane, eventually, leading to a compromise between the mechanical strength and ionic conductivity. Figure 3b displays the TG and DSC curves of the TPU and ATO-TPU membranes. The decomposition temperature of the TPU and ATO-TPU membrane is about 300°C , which could satisfy the safety requirement of LIBs. No notable endothermic peak can be seen before 300°C for the TPU and ATO-TPU membranes, while the commercial separator shows two characteristic endothermic peaks at 146.58°C and 486.16°C (Fig.S1b), relating to the melting and decomposition of PP, respectively. The crystallinity of PP calculated from DSC analysis is $\sim 68.5\%$. As a comparison, the crystallinity of TPU and ATO-TPU membranes is $\sim 45.6\%$ and 41.5% , respectively. The thermal shrinkage of the membranes was estimated by measuring their change in size after being submitted to heat treatment at various temperatures for 0.5 h. As can be seen from Fig. 3c, the TPU and ATO-TPU membranes exhibit excellent thermal stability up to 180°C , while the PP membrane undergoes impressive shrinkage with the color varying from white to transparent at 180°C , indicating the TPU

Figure 2 SEM images of **a** and **b** TPU, **c** and **d** ATO-TPU membranes. **e** SEM image of the analyzed area, **f** the corresponding elements (C, O, Ti and N) mapping of the selected area.

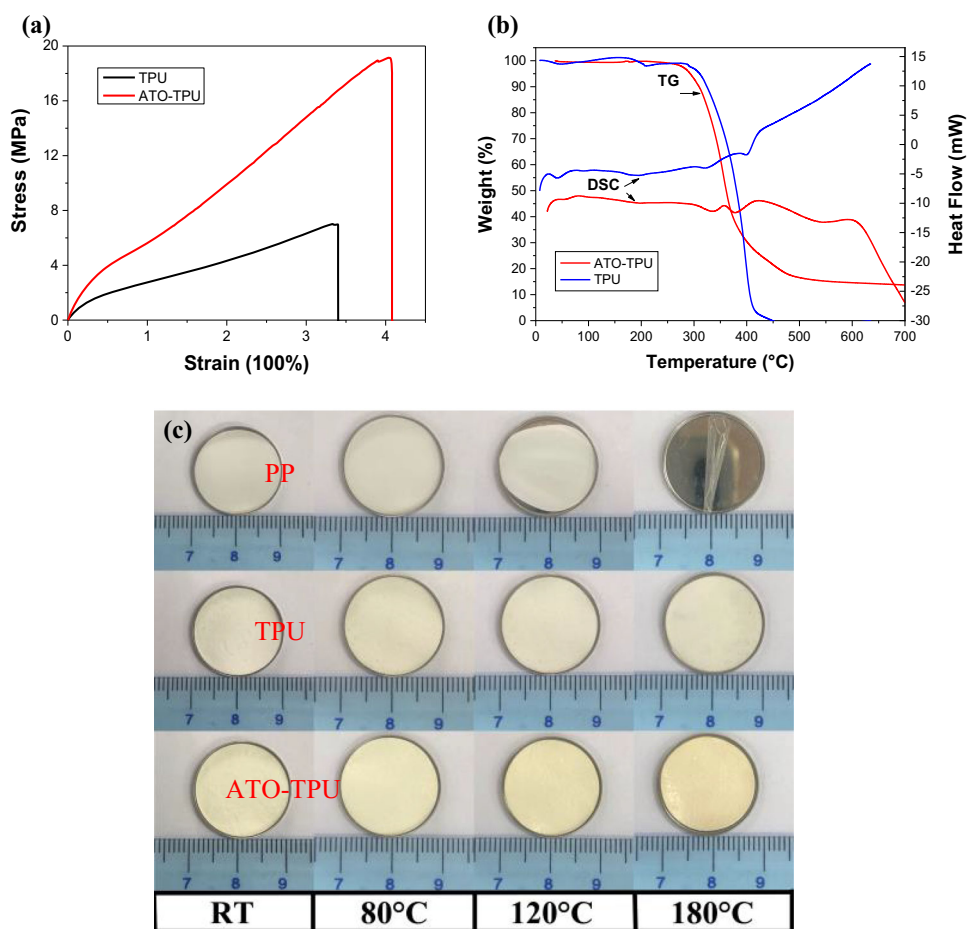


and ATO-TPU membranes have better thermal stability than the PP membrane.

Sufficient electrolyte uptake is necessary to provide high ion conductivity in GPEs. The liquid electrolyte uptake capability of the PP, TPU and ATO-TPU membranes is displayed in Fig. 4a, b. The enlarged area of the ATO-TPU membrane after uptaking liquid electrolyte is significantly higher than that of the PP membrane. The ATO-TPU membrane exhibits an electrolyte uptake of 259%, which guarantees the high ionic conductivity. The AC impedance results of PP, TPU and ATO-TPU GPEs are shown in Fig. 4c. The ATO-TPU GPE exhibits an ionic conductivity of 1.59 mS cm^{-1} at 25°C , which can be attributed to the unique blending structure of TPU and the lipophilicity of TiO_2 [24, 41]. In addition, the

interaction of nanoparticles with the polymer hinders the polymer chain organization [45]. Low crystallization is favorable for enhancing the ionic conductivity of the polymer electrolyte [46, 47]. In contrast, the PP separator shows a low electrolyte uptake of 72% and further exhibits an ionic conductivity of 0.56 mS cm^{-1} at 25°C . The temperature dependence of ionic conductivity of PP, TPU and ATO-TPU is illustrated in Fig. 4d. In the temperature regime between 20° and 80°C , the ionic conductivity increases linearly with the temperature, which is consistent with the Arrhenius relationship. Linear sweep voltammetry (LSV) was used to measure the electrochemical stability of the separators and GPEs. Figure 4e displays the electrochemical stability of PP, TPU and ATO-TPU GPE. The ATO-TPU GPE shows

Figure 3 **a** Stress–strain curves of the TPU and ATO-TPU membranes. **b** The TG/DSC curves of TPU and ATO-TPU. **c** Thermal stability tests of PP, TPU and ATO-TPU membranes.



good oxide stability up to 4.3 V. With the voltage over 4.3 V, the current firstly increases and then decreases rapidly, which can be ascribed to the reversible Li deposition on the surface of stainless steel electrode [48, 49]. After that, the subsequent increase in current is associated with the decomposition of electrolytes [50, 51]. Compared with PP, the TPU matrix greatly increases the decomposition voltage of the electrolytes in the GPE. The results indicate that the ATO-TPU GPE can be compatible with most of the cathode materials. The Li^+ transference number (t_{Li^+}) is pivotal for the electrochemical performance of LIBs. The t_{Li^+} of PP, TPU and ATO-TPU GPEs obtained by chronoamperometry combined with EIS tests is shown in Fig. 4f and Fig.S2. As summarized in Table S1, obviously, the t_{Li^+} of ATO-TPU GPE was much higher than that of PP and TPU GPE. Due to the strong interaction between the polyurethane and polar electrolyte solvents, high electrolyte uptake can be obtained in TPU-based GPE, which can promote the Li-ion diffusion in GPE.

The interconnected pores created by the lipophilic TiO_2 nanoparticles provide abundant channels for ion transport. As shown in Table S2, the addition of ceramic filler to the polymer matrix creates space charge layer at the filler–polymer interface which assists in ion transport [19]. Besides, TiO_2 nanoparticles create localized amorphous regions in TPU matrix and thus enhance the Li^+ ions transport in the amorphous polymer electrolyte.

The charge/discharge profiles of the testing cells with PP separator, TPU and ATO-TPU GPEs in the first cycle are depicted in Fig. 5a. The testing cell with the ATO-TPU GPE delivers the highest discharge capacity at 0.2 C rate and 25 °C. The cycling performance of the testing cells was evaluated by measuring the discharge capacity operating at 0.2 C for both charge and discharge in the same potential range (Fig. 5c). The testing cell with ATO-TPU GPE shows excellent cycling performance up to 100 cycles than the PP and TPU GPE, which can be ascribed to its good compatibility toward liquid electrolyte.

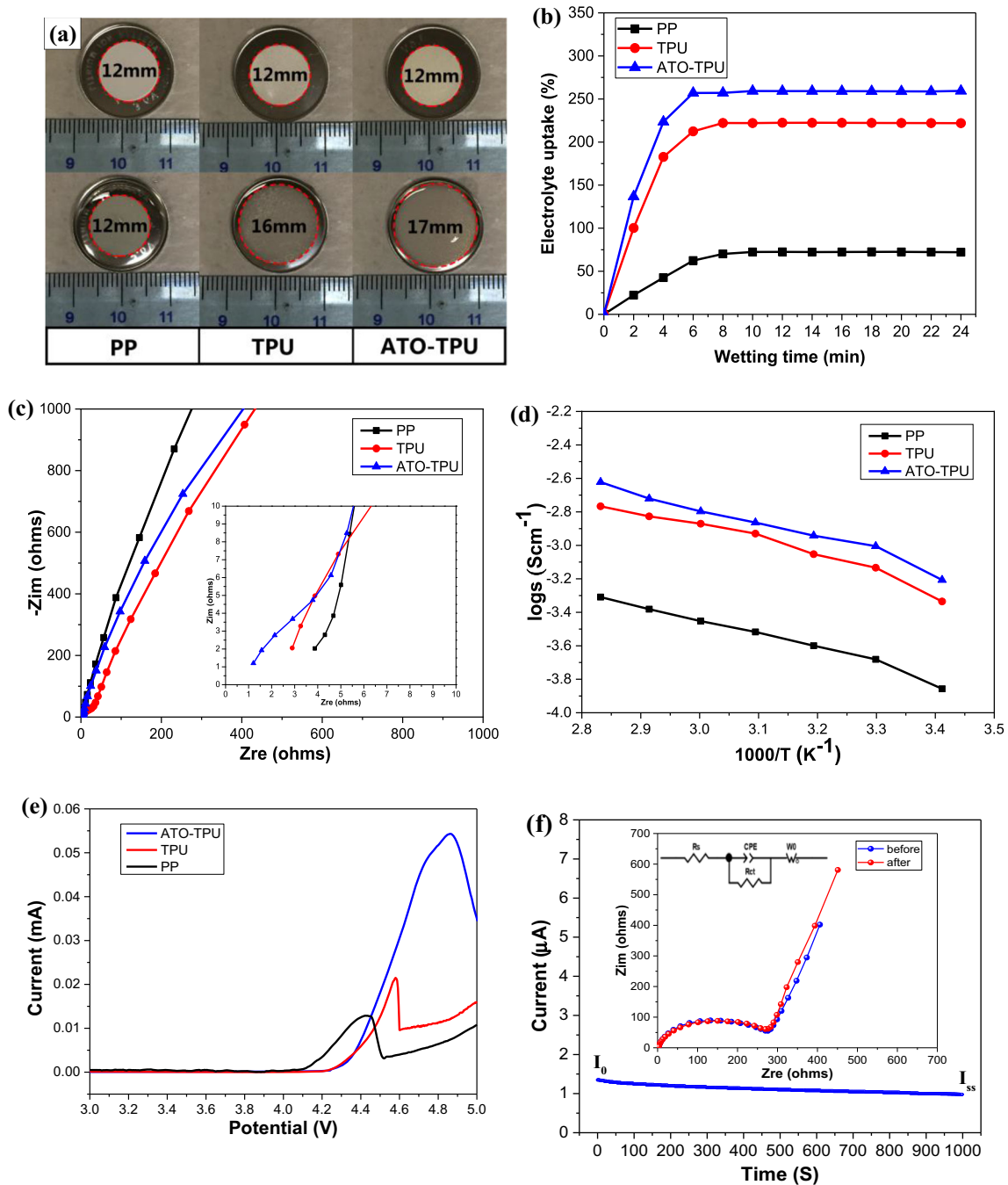


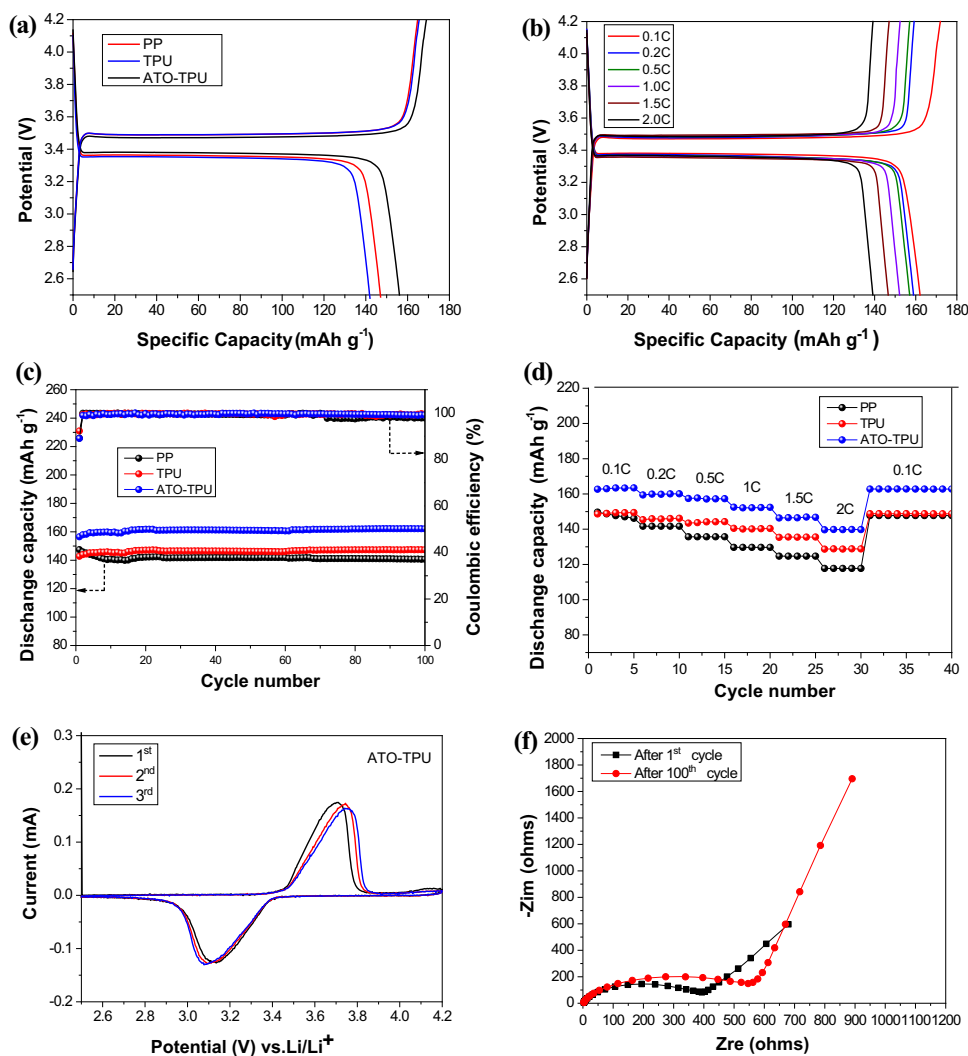
Figure 4 **a** Liquid electrolyte wettability of the TPU and ATO-TPU membranes measured by soaking in liquid electrolyte for 10 min. **b** Electrolyte uptake of the TPU and ATO-TPU membranes. **c** AC impedance spectra of the PP, TPU and ATO-TPU GPEs in stainless steel/GPE/stainless steel system. **d** Ionic

conductivity of the PP, TPU and ATO-TPU GPEs at different temperatures. **e** Electrochemical stability of the PP, TPU and ATO-TPU GPEs. **f** Chronoamperometry profiles and AC impedance analyses of Li/GPE/Li cell with ATO-TPU GPE.

Figure 5b and Fig.S3 depict the charge/discharge curves of LIBs with PP, TPU and ATO-TPU GPEs at different C-rates. In Fig.S3, the testing cell with PP separator exhibits a discharge capacity of

141 mAh g⁻¹ and 117 mAh g⁻¹ at 0.2 C and 2 C, respectively. By contrast, a remarkable increase in discharge capacities of the cell assembled with ATO-TPU GPE at 0.2 C can be observed. The cell with

Figure 5 Electrochemical behavior of the PP, TPU and ATO-TPU GPE. **a** Charge–discharge performance at the 1st cycle. **b** Charge–discharge performance of test cell with ATO-TPU GPE at different C-rates. **c** Cycling performance of the testing cells at 0.2 C. **d** Cycle capability of the testing cells at various C-rates. **e** CV measurements of the cells with ATO-TPU GPE. **f** EIS profiles of the cells with ATO-TPU GPE after 1st and 100th cycles.



ATO-TPU GPE can deliver a high discharge capacity of 137 mAh g^{-1} even at a rate of 2.0 C. Besides, the voltage plateau in the charge/discharge curves of the cell with ATO-TPU GPE at different rates is highly overlapped, indicating the polarization can be neglected. As clearly shown in Fig. 5d, the cell with ATO-TPU GPE exhibits enhanced rate capability from 0.1 to 2.0 C compared with the cells with PP separator and TPU GPE. The enhanced rate capability of ATO-TPU GPE can be mainly attributed to the high ionic conductivity.

CV curves of the testing cell with ATO-TPU GPE in the first three cycles are presented in Fig. 5e. A set of symmetrical and sharp anodic/cathodic peaks can be observed, which indicates excellent electrochemical reversibility in the cycling. AC impedance spectra of the fully charged cells after the 1st and 100th cycles were measured (Fig. 5f, Fig.S4 and Fig.S5). It can be

concluded that ATO-TPU GPE strongly hampers the increase in the electrochemical reaction resistance.

Schematic diagrams of the testing cells with PP and ATO-TPU GPE are shown in Fig. 6a, b, respectively. As far as we know, Li dendrites grew in an uncontrollable manner may penetrate through the PP separator and result in the inner short circuit of the cells. Thus, the double-side coating method has been employed to improve the mechanical properties and thermal stability of the commercial separators. In this work, the ATO nanoparticles in TPU GPE can effectively resist the penetration of Li dendrites due to the high crystallinity and stiffness of ATO. A Li/Li symmetric cell was assembled with ATO-TPU GPE to evaluate the effect of ATO-TPU GPE on suppression of Li dendrite growth. As shown in Fig. 6c, a relatively high overpotential can be observed over the first few tens of hours for the PP, TPU and ATO-TPU

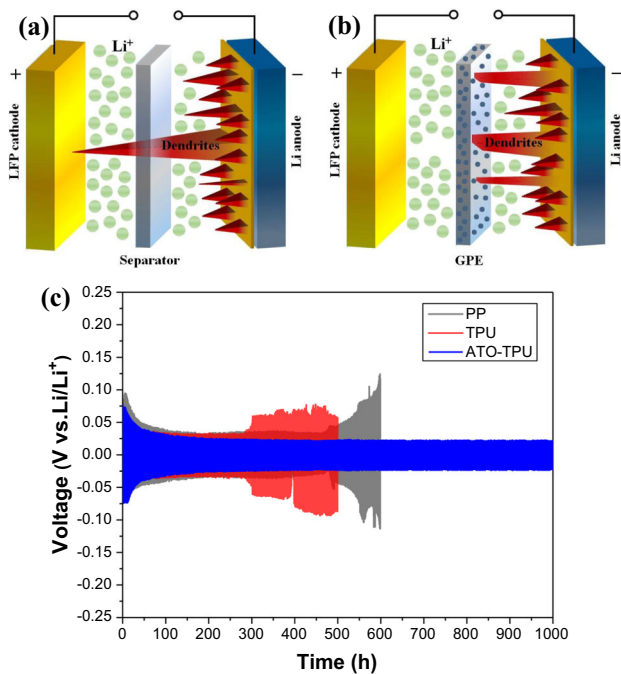


Figure 6 Schematic diagrams of the testing cells with PP separator (a) and ATO-TPU GPE (b). c Voltage–time profile of Li/Li symmetric cells assembled with PP, TPU and ATO-TPU GPE at 0.2 mA cm^{-2} with a capacity of 0.2 mAh cm^{-2} .

GPE due to the activation and increasing surface area in the cathode during the Li stripping/plating process. For the cell assembled with PP separator, a stable potential can be obtained in the range of 100 h to 450 h. After 450 h, the testing cell shows a fluctuation in the potential, which was caused by the uncontrollable growth of Li dendrites and the short circuit from the destruction of PP separators. The cell with TPU GPE is more susceptible to the Li dendrites growth due to the low strength of TPU GPE. Testing cell assembled with ATO-TPU GPE showed high potential stability up to 1000 h, indicating that the ATO-TPU GPE has higher strength than the PP and TPU GPE.

The cycling performance of the testing Li/LiFePO₄ cells with PP, TPU and ATO-TPU GPE at a high temperature of 60 °C was further investigated. As shown in Fig. 7, a capacity fluctuation is observed in the cell assembled with PP separator in 50 cycles. Good cycling performance can be obtained in the cell with ATO-TPU GPE. The specific discharge capacities at 1st and 50th cycles are 145 mAhg^{-1} and 139 mAhg^{-1} , respectively, with a capacity retention of 95%. The electrochemical behavior of the testing cell is consistent with the results shown in Fig. 4d.

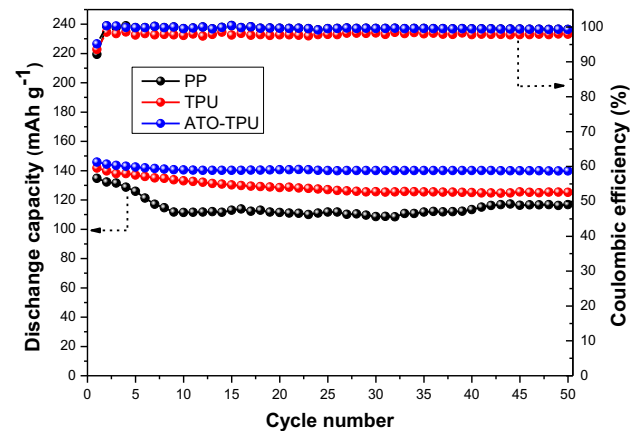


Figure 7 Cycling performance of the testing Li/LiFePO₄ cells with the PP, TPU and ATO-TPU GPE at a high temperature of 60 °C.

The ATO-TPU GPE has a potential for wide-scale application in high-temperature LIBs due to its high ionic conductivity, good thermal stability and high resistance toward Li dendrite growth.

Conclusion

GPE based on TPU and ATO was successfully prepared by an easy phase separation technique. ATO-TPU GPE exhibits superior thermal stability, high strength and excellent interface stability to lithium metal electrode. ATO-TPU GPE displays lower voltage polarization and longer valid cycle life than the conventional liquid electrolyte. The testing cell with ATO-TPU GPE shows excellent cycling performance and rate capability with nearly 100% Coulombic efficiency in the first 100 cycles. Besides, good electrochemical performance can be achieved at a high temperature of 60 °C. The results indicate that ATO-TPU GPE could be a promising candidate for LIBs with higher safety.

Acknowledgements

This work was financially supported by the National Natural Science Foundation of China (No. 51702371), High-level Talent Gathering Project in Hunan Province (2019RS1059), Graduate Innovation Foundation of Hunan Province (Nos. 2018XTUXJ049 and 201810530017) and Postgraduate Education Reform Project of Hunan Province (Grant Nos. CX20190423).

Data availability

The authors declare that the data supporting the findings of this study are available within the article and its Supplementary Information files.

Compliance with ethical standards

Conflict of interest The authors declare no conflict of interest.

Electronic supplementary material: The online version of this article (<https://doi.org/10.1007/s10853-020-05360-5>) contains supplementary material, which is available to authorized users.

References

- [1] Chen H, Zhang W, Tang X-Q, Ding Y-H, Yin J-R, Jiang Y, Zhang P, Jin H (2018) First principles study of P-doped borophene as anode materials for lithium ion batteries. *Appl Surf Sci* 427:198–205. <https://doi.org/10.1016/j.apsusc.2017.08.178>
- [2] Guo L-F, Zhang S-Y, Xie J, Zhen D, Jin Y, Wan K-Y, Zhuang D-G, Zheng W-Q, Zhao X-B (2020) Controlled synthesis of nanosized Si by magnesiothermic reduction from diatomite as anode material for Li-ion batteries. *Int J Miner Metall Mater* 27:515–525. <https://doi.org/10.1007/s12613-019-1900-z>
- [3] Setiawan H, Petrus HTBM, Perdana I (2019) Reaction kinetics modeling for lithium and cobalt recovery from spent lithium-ion batteries using acetic acid. *Int J Miner Metall Mater* 26:98–107. <https://doi.org/10.1007/s12613-019-1713-0>
- [4] Li Y, Cheng L-N, Miao W-K, Wang C-X, Kuang D-Z, Han S-M (2020) Nd–Mg–Ni alloy electrodes modified by reduced graphene oxide with improved electrochemical kinetics. *Int J Miner Metall Mater* 27:391–400. <https://doi.org/10.1007/s12613-019-1880-z>
- [5] Tang W, Zhu Y, Hou Y, Liu L, Wu Y, Loh KP, Zhang H, Zhu K (2013) Aqueous rechargeable lithium batteries as an energy storage system of superfast charging. *Energy Environ Sci* 6:2093–2104. <https://doi.org/10.1039/C3EE24249H>
- [6] Sun J, Lu C, Tian Q, Mei Y, Peng J, Ding Y (2020) V₂O₃/MoS₂ microspheres as a high-performance anode for Li-storage. *Appl Surf Sci* 513:145756. <https://doi.org/10.1016/j.apsusc.2020.145756>
- [7] Jiang W, Liu Q, Peng J, Jiang Y, Ding Y, Wei Q (2020) Co₉S₈ nanoparticles embedded into amorphous carbon as anode materials for lithium-ion batteries. *Nanotechnology* 31:235713. <https://doi.org/10.1088/1361-6528/ab7887>
- [8] Zhang W, Yin J, Zhang P, Tang X, Ding Y (2018) Two-dimensional phosphorus carbide as a promising anode material for lithium-ion batteries. *J Mater Chem A* 6:12029–12037. <https://doi.org/10.1039/C8TA02995D>
- [9] Zhu J, Wierzbicki T, Li W (2018) A review of safety-focused mechanical modeling of commercial lithium-ion batteries. *J Power Sources* 378:153–168. <https://doi.org/10.1016/j.jpowsour.2017.12.034>
- [10] Jiang Y, Zhang P, Jin H, Liu X, Ding Y (2019) Flexible, nonflammable and Li-dendrite resistant Na₂Ti₃O₇ nanobelt-based separators for advanced Li storage. *J Membr Sci* 583:190–199. <https://doi.org/10.1016/j.memsci.2019.04.032>
- [11] Deng C, Jiang Y, Fan Z, Zhao S, Ouyang D, Tan J, Zhang P, Ding Y (2019) Sepiolite-based separator for advanced Li-ion batteries. *Appl Surf Sci* 484:446–452. <https://doi.org/10.1016/j.apsusc.2019.04.141>
- [12] Cheng X, Pan J, Zhao Y, Liao M, Peng H (2018) Gel polymer electrolytes for electrochemical energy storage. *Adv Energy Mater* 8:1702184. <https://doi.org/10.1002/aenm.201702184>
- [13] Kuo P-L, Tsao C-H, Hsu C-H, Chen S-T, Hsu H-M (2016) A new strategy for preparing oligomeric ionic liquid gel polymer electrolytes for high-performance and non-flammable lithium ion batteries. *J Membr Sci* 499:462–469. <https://doi.org/10.1016/j.memsci.2015.11.007>
- [14] Kalyana Sundaram NT, Vasudevan T, Subramania A (2007) Synthesis of ZrO₂ nanoparticles in microwave hydrolysis of Zr (IV) salt solutions—Ionic conductivity of PVdF-co-HFP-based polymer electrolyte by the inclusion of ZrO₂ nanoparticles. *J Phys Chem Solids* 68:264–271. <https://doi.org/10.1016/j.jpcs.2006.11.005>
- [15] Xiang H, Chen J, Li Z, Wang H (2011) An inorganic membrane as a separator for lithium-ion battery. *J Power Sources* 196:8651–8655. <https://doi.org/10.1016/j.jpowsour.2011.06.055>
- [16] Liu Q, Jiang W, Lu W, Mei Y, He F, Zhang M, Liu Y, Chen Y, Peng J, Ding Y (2020) Anisotropic semi-aligned PAN@PVdF-HFP separator for Li-ion batteries. *Nanotechnology* 31:435701. <https://doi.org/10.1088/1361-6528/aba303>
- [17] Jiang Y, Ding Y, Zhang P, Li F, Yang Z (2018) Temperature-dependent on/off PVP@TiO₂ separator for safe Li-storage. *J Membr Sci* 565:33–41. <https://doi.org/10.1016/j.memsci.2018.08.008>
- [18] Yin J, Wu B, Wang Y, Li Z, Yao Y, Jiang Y, Ding Y, Xu F, Zhang P (2018) Novel elastic, lattice dynamics and thermodynamic properties of metallic single-layer transition

- metal phosphides: 2H–M2P (Mo2P, W2P, Nb2P and Ta2P). *J Phys: Condens Matter* 30:135701
- [19] Kumar R, Subramania A, Sundaram NTK, Kumar GV, Baskaran I (2007) Effect of MgO nanoparticles on ionic conductivity and electrochemical properties of nanocomposite polymer electrolyte. *J Membr Sci* 300:104–110. <https://doi.org/10.1016/j.memsci.2007.05.014>
- [20] Priya ARS, Subramania A, Jung Y-S, Kim K-J (2008) High-performance quasi-solid-state dye-sensitized solar cell based on an electrospun PVdF–HFP membrane electrolyte. *Langmuir* 24:9816–9819. <https://doi.org/10.1021/la801375s>
- [21] Subramania A, Kalyana Sundaram NT, Sathiyapriya AR, Vijaya Kumar G (2007) Preparation of a novel composite micro-porous polymer electrolyte membrane for high performance Li-ion battery. *J Membr Sci* 294:8–15. <https://doi.org/10.1016/j.memsci.2007.01.025>
- [22] Sundaram NTK, Musthafa OTM, Lokesh KS, Subramania A (2008) Effect of porosity on PVdF-co-HFP–PMMA-based electrolyte. *Mater Chem Phys* 110:11–16. <https://doi.org/10.1016/j.matchemphys.2007.12.024>
- [23] Jin H, Ding Y-H, Wang M, Song Y, Liao Z, Newcomb CJ, Wu X, Tang X-Q, Li Z, Lin Y, Yan F, Jian T, Mu P, Chen C-L (2018) Designable and dynamic single-walled stiff nanotubes assembled from sequence-defined peptoids. *Nature Communications* 9:270. <https://doi.org/10.1038/s41467-017-02059-1>
- [24] Yarmolenko OV, Yudina AV, Khatmullina KG (2018) Nanocomposite polymer electrolytes for the lithium power sources (a Review). *Russ J Electrochem* 54:325–343. <https://doi.org/10.1134/S1023193518040092>
- [25] Lu Q, Yang J, Lu W, Wang J, Nuli Y (2015) Advanced semi-interpenetrating polymer network gel electrolyte for rechargeable lithium batteries. *Electrochim Acta* 152:489–495. <https://doi.org/10.1016/j.electacta.2014.11.176>
- [26] Li H, Li M, Siyal SH, Zhu M, Lan J-L, Sui G, Yu Y, Zhong W, Yang X (2018) A sandwich structure polymer/polymer-ceramics/polymer gel electrolytes for the safe, stable cycling of lithium metal batteries. *J Membr Sci* 555:169–176. <https://doi.org/10.1016/j.memsci.2018.03.038>
- [27] Zhu M, Wu J, Zhong W-H, Lan J, Sui G, Yang X (2018) A biobased composite gel polymer electrolyte with functions of lithium dendrites suppressing and manganese ions trapping. *Adv Energy Mater* 8:1702561. <https://doi.org/10.1002/aenm.201702561>
- [28] Zhang Y, Zhao Y, Cheng X, Weng W, Ren J, Fang X, Jiang Y, Chen P, Zhang Z, Wang Y, Peng H (2015) Realizing both high energy and high power densities by twisting three carbon-nanotube-based hybrid fibers. *Angew Chem Int Ed* 54:11177–11182. <https://doi.org/10.1002/anie.201506142>
- [29] Takeda Y, Yamamoto O, Imanishi N (2016) Lithium dendrite formation on a lithium metal anode from liquid, polymer and solid electrolytes. *Electrochemistry* 84:210–218. <https://doi.org/10.5796/electrochemistry.84.210>
- [30] Lu Q, He Y-B, Yu Q, Li B, Kaneti YV, Yao Y, Kang F, Yang Q-H (2017) Dendrite-free, high-rate, long-life lithium metal batteries with a 3D cross-linked network polymer electrolyte. *Adv Mater* 29:1604460. <https://doi.org/10.1002/adma.201604460>
- [31] Wu H, Cao Y, Su H, Wang C (2018) Tough gel electrolyte using double polymer network design for the safe, stable cycling of lithium metal anode. *Angew Chem Int Ed* 57:1361–1365. <https://doi.org/10.1002/anie.201709774>
- [32] Wang Y, Liu B, Li Q, Cartmell S, Ferrara S, Deng ZD, Xiao J (2015) Lithium and lithium ion batteries for applications in microelectronic devices: a review. *J Power Sources* 286:330–345. <https://doi.org/10.1016/j.jpowsour.2015.03.164>
- [33] Liang S, Yan W, Wu X, Zhang Y, Zhu Y, Wang H, Wu Y (2018) Gel polymer electrolytes for lithium ion batteries: fabrication, characterization and performance. *Solid State Ion* 318:2–18. <https://doi.org/10.1016/j.ssi.2017.12.023>
- [34] Yang D, He L, Liu Y, Yan W, Liang S, Zhu Y, Fu L, Chen Y, Wu Y (2019) An acetylene black modified gel polymer electrolyte for high-performance lithium–sulfur batteries. *J Mater Chem A* 7:13679–13686. <https://doi.org/10.1039/C9TA03123E>
- [35] Zhu Y, Xiao S, Shi Y, Yang Y, Wu Y (2013) A trilayer poly(vinylidene fluoride)/polyborate/poly(vinylidene fluoride) gel polymer electrolyte with good performance for lithium ion batteries. *J Mater Chem A* 1:7790–7797. <https://doi.org/10.1039/C3TA00167A>
- [36] Liang S, Shi Y, Ma T, Yan W, Qin S, Wang Y, Zhu Y, Wang H, Wu Y (2019) A compact gel membrane based on a blend of PEO and PVDF for dendrite-free lithium metal anodes. *ChemElectroChem* 6:5413–5419. <https://doi.org/10.1002/celec.201901351>
- [37] Chen W-C, Chen H-H, Wen T-C, Digar M, Gopalan A (2004) Morphology and ionic conductivity of thermoplastic polyurethane electrolytes. *J Appl Polym Sci* 91:1154–1167. <https://doi.org/10.1002/app.13208>
- [38] Tian L-y, Zhu W-h, Tang X (2003) Polymer gel electrolytes based on thermoplastic polyurethane. *J Appl Polym Sci* 90:2310–2315. <https://doi.org/10.1002/app.12732>
- [39] Liu X, Song K, Lu C, Huang Y, Duan X, Li S, Ding Y (2018) Electrospun PU@GO separators for advanced lithium ion batteries. *J Membr Sci* 555:1–6. <https://doi.org/10.1016/j.memsci.2018.03.027>
- [40] Song K, Zhang P, Huang Y, Xu F, Ding Y (2019) Electrospun PU/PVP/GO separator for Li-ion batteries. *Fibers*

- Polym 20:961–965. <https://doi.org/10.1007/s12221-019-8883-2>
- [41] Wu N, Jing B, Cao Q, Wang X, Kuang H, Wang Q (2012) A novel electrospun TPU/PVdF porous fibrous polymer electrolyte for lithium ion batteries. *J Appl Polym Sci* 125:2556–2563. <https://doi.org/10.1002/app.36523>
- [42] Kim BG, Kim J-S, Min J, Lee Y-H, Choi JH, Jang MC, Freunberger SA, Choi JW (2016) A moisture- and oxygen-impermeable separator for aprotic Li–O₂ batteries. *Adv Funct Mater* 26:1747–1756. <https://doi.org/10.1002/adfm.201504437>
- [43] Zhou L, Cao Q, Jing B, Wang X, Tang X, Wu N (2014) Study of a novel porous gel polymer electrolyte based on thermoplastic polyurethane/poly(vinylidene fluoride-co-hexafluoropropylene) by electrospinning technique. *J Power Sources* 263:118–124. <https://doi.org/10.1016/j.jpowsour.2014.03.140>
- [44] Karthick SN, Prabakar K, Subramania A, Hong J-T, Jang J-J, Kim H-J (2011) Formation of anatase TiO₂ nanoparticles by simple polymer gel technique and their properties. *Powder Technol* 205:36–41. <https://doi.org/10.1016/j.powtec.2010.08.061>
- [45] Maurya DK, Murugadoss V, Angaiah S (2019) All-solid-state electrospun poly(vinylidene fluoride-co-hexafluoropropylene)/Li_{7.1}La₃Ba_{0.05}Zr_{1.95}O₁₂ nanohybrid membrane electrolyte for high-energy Li-ion capacitors. *J Phys Chem C* 123:30145–30154. <https://doi.org/10.1021/acs.jpcc.9b09264>
- [46] Solarajan AK, Murugadoss V, Angaiah S (2017) High performance electrospun PVdF-HFP/SiO₂ nanocomposite membrane electrolyte for Li-ion capacitors. *J Appl Polym Sci* 134:45177. <https://doi.org/10.1002/app.45177>
- [47] Solarajan AK, Murugadoss V, Angaiah S (2016) Montmorillonite embedded electrospun PVdF–HFP nanocomposite membrane electrolyte for Li-ion capacitors. *Appl Mater Today* 5:33–40. <https://doi.org/10.1016/j.apmt.2016.09.002>
- [48] Liu F-Q, Wang W-P, Yin Y-X, Zhang S-F, Shi J-L, Wang L, Zhang X-D, Zheng Y, Zhou J-J, Li L, Guo Y-G (2018) Upgrading traditional liquid electrolyte via in situ gelation for future lithium metal batteries. *Sci Adv* 4:eaat5383. <https://doi.org/10.1126/sciadv.aat5383>
- [49] Khani H, Kalami S, Goodenough JB (2020) Micropores-in-macroporous gel polymer electrolytes for alkali metal batteries. *Sustain Energy Fuels* 4:177–189. <https://doi.org/10.1039/C9SE00690G>
- [50] Syahidah SN, Majid SR (2013) Super-capacitive electrochemical performance of polymer blend gel polymer electrolyte (GPE) in carbon-based electrical double-layer capacitors. *Electrochim Acta* 112:678–685. <https://doi.org/10.1016/j.electacta.2013.09.008>
- [51] Jin J, Wen Z, Liang X, Cui Y, Wu X (2012) Gel polymer electrolyte with ionic liquid for high performance lithium sulfur battery. *Solid State Ion* 225:604–607. <https://doi.org/10.1016/j.ssi.2012.03.012>

Publisher's Note Springer Nature remains neutral with regard to jurisdictional claims in published maps and institutional affiliations.